Bénard-Marangoni convective patterns in small cylindrical layers

T. Ondarçuhu,* J. Millán-Rodríguez, H. L. Mancini,† A. Garcimartín, and C. Pérez-García‡
Departamento de Física y Matemática Aplicada, Facultad de Ciencias, Universidad de Navarra, E-31080 Pamplona, Navarra, Spain
(Received 23 November 1992)

A study of Bénard-Marangoni convection in containers of small aspect ratio (defined as the ratio of the diameter of the container to the depth of the liquid) is presented. In this situation, sidewall constraints have an important role in selecting the pattern at the onset of convection. In many situations, this pattern is axisymmetric with well-distributed azimuthal nodal lines (simple mode). When increasing an external parameter (supercritical heating), more complex dynamics can appear due to secondary instabilities. The experimental results presented here show that patterns beyond threshold can be just simple modes, a linear combination of simple modes, or more complicated structures that cannot be described just by superposition of a few modes. These experimental results are compared with some theoretical models, based on amplitude equations, and on a generalized Swift-Hohenberg equation. Whereas the former approach provides a simple and straightforward description for certain patterns near threshold, simulations of the latter give many of the patterns observed in the experiments.

PACS number(s): 47.27.Te, 47.20.Dr

I. INTRODUCTION

Bénard-Marangoni (BM) convection arises when a liquid layer with an upper free surface is heated from below. If the temperature difference between the bottom and top surfaces exceeds a threshold value ΔT_c, the conductive state loses stability and the convective state appears. In the BM case the instability mechanism is a combination of buoyancy and surface-tension variation with temperature [1]. The threshold value ΔT_c can be derived from the linearized basic equations, as well as the critical wave number k_c, after applying the Oberbeck-Boussinesq approximation [1].

Above threshold, a nonlinear analysis allows one to determine the stable pattern. In the case of BM instability, the pattern is formed of hexagonal cells, as reported in the old experiments of Bénard [2], and more recently by Koschmieder [3] and Cerisier *et al.* [4]. A weakly nonlinear theoretical analysis was undertaken by Scanlon and Segel [5] for a quite idealized situation (infinite depth, no buoyancy effects), and by Cloot and Lebon [6]. These analyses confirm that the pattern of hexagons is stable in BM convection. Near threshold the pattern can have some defects, but it is almost stationary. However, when the temperature difference is increased further the number of defects is higher and the pattern becomes time dependent [3,4,7].

Those experiments were performed in containers of large aspect ratio Γ (which is the ratio of the diameter to the depth of the fluid) and in the theoretical works a layer of infinite horizontal extent was considered. However, it is interesting to examine the case of small Γ, where the convective pattern is dominated by sidewall constraints. Lateral boundaries restrict the continuous spectrum of wave vectors allowed in a linear analysis of the infinite case to one or a few competing modes. This has been made for the Rayleigh-Bénard instability (liquid confined between two rigid plates), where the Feigenbaum cascade and other routes to chaos were observed in small-aspect-ratio rectangular containers [8,9].

The most relevant theoretical work for small-aspect-ratio BM convection is due to Rosenblat, Davis, and Homsy [10] (to whom we will refer as RDH in the following), who considered the case of a liquid layer bounded by cylindrical lateral walls. These walls are frictionless, so that the usual nonslip condition is replaced by the condition of zero tangential vorticity. Although this is a strong idealization, it allows a mathematical simplification because a separation of variables can be carried out. In these calculations the Rayleigh number R is assumed to be zero. The solution for the vertical velocity component near threshold is expanded in simple modes as

$$v(r,\theta,z)=\sum_{i,j,m} A_{ijm} J_m(\lambda_{mi} r)\cos(m\theta) f_{ijm}(z) ,$$

where m is an integer giving the azimuthal wave number, J_m is a Bessel function with an appropriate radial wave number λ_{mi}, $f_{ijm}(z)$ are the eigenfunctions of the linear analysis of the balance equations governing the phenomena, and A_{ijm} are the time-dependent amplitudes. These solutions describe convective cells that are concentric circles with azimuthal nodal lines.

Performing a weakly nonlinear analysis, these authors examined the dynamics of the amplitudes A_{mij} of the simple modes (amplitude equations) that occur as Γ and the supercriticality ϵ [defined as $\epsilon=(\Delta T-\Delta T_c)/\Delta T_c$] are changed. When increasing ϵ for a fixed Γ, they predicted transitions between simple modes and a linear combination of simple modes (mixed modes). For most aspect ratios, this gives quite simple behaviors described by amplitude equations corresponding to supercritical transitions. More complicated scenarios are found for those aspect ratios where two simple modes lose stability simultaneously. The nonlinear interaction of these modes can result in a quite complex series of transitions. These

higher instabilities may give rise to hysteresis effects, jump phenomena, or time-dependent convection. This constitutes a very rich scenario which has not yet been experimentally examined.

Some experiments with small aspect ratio containers have been carried out. Cerisier *et al.* [11] showed the stability of a single hexagon surrounded by polygons for $\Gamma=8.2$. These authors also showed that the hexagon size relaxed to a natural value after a perturbation is applied. Koschmieder and Prahl [12] restricted themselves to the observation of patterns near threshold. They showed the existence of simple modes predicted by RHD, but the order of appearance is not the one predicted by the theoretical work. They also verified that the marginal curve predicted by RDH agrees quite well with their measurements. In those experiments, a regular increase of the number of cells is observed as Γ is enlarged. Ezersky, Preobrazhensky, and Rabinovich [13] found a similar behavior in convection with inhomogeneous heating. In these two last experiments, a central hexagon is also obtained for Γ large enough. (Notice that this form is not describable by a superposition of a few simple modes.)

The main aim of the present work is to determine the different kinds of patterns and transitions obtained when the two main parameters ϵ and Γ are changed. We present experimental results and compare them with some theoretical descriptions. The amplitude equation formalism assumes a perfectly symmetric pattern and so it can succeed in describing simple or mixed modes, but it cannot deal with more general patterns. This limitation can be avoided with the Swift-Hohenberg approach [14,15], which gives a model equation by which complicated patterns can be described.

This paper is organized as follows. The characteristics of the container and the experimental setup are described in Sec. II. In Sec. III the different features of the patterns obtained in the experiments are shown. Section IV is devoted to the numerical simulations performed with a generalized Swift-Hohenberg (GSH) model. Finally, a comparison between the experimental results and numerical simulations is presented with some conclusions in Sec. V.

II. EXPERIMENTAL SETUP

The experimental setup is sketched in Fig. 1. The container, made of aluminium, has a diameter of 120 mm. A 68-mm-diam nylon ring of calibrated width is placed inside the container, and this is the lateral wall of the region we observe. The container is filled so that the height of the liquid reaches the rim of the ring. In this way the surface of the fluid is almost undisturbed by meniscus effects. The horizontal gradient in the walls is also minimized: there is liquid at approximately the same temperature on both sides, and the thermal conductivity of nylon is not far from that of the 350 cS silicone oil employed. We used a set of rings with different heights (from 8 to 17 mm) in order to cover a wide range of aspect ratios.

The depth of the liquid layer is measured very precisely using a thin probe driven by a microcontroller that allows to move it in 1-μm vertical steps. The contact of the probe with the free surface is easily detected because a meniscus is suddenly formed. The bottom of the container is detected by measuring the electrical resistance between it and the probe. The measurement can be made with a precision of few microns at each point, but the roughness of the whole cell amounts for some tens of microns.

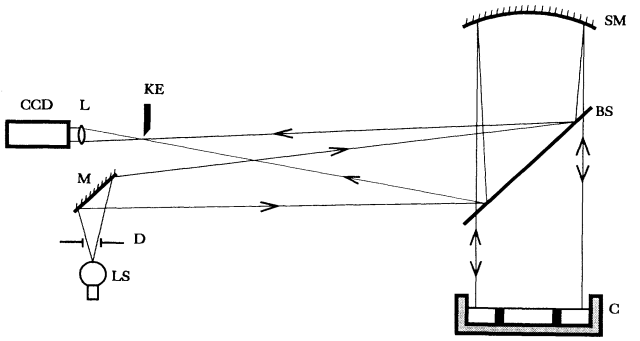

FIG. 1. Sketch of the experimental setup. LS, light source; D, diaphragm; M, mirror; BS, beam splitter; SM, spherical mirror; C, container; KE, knife edge; L, lens; CCD, standard CCD camera.

The aluminum container is placed on a thick copper block heated from below by an electrical resistance with controlled power supply. The upper surface of the liquid is in contact with air. A refrigerating system can be used but it renders observation more difficult, and as long as it does not give significant changes in the patterns we did not use it to obtain the results shown here. The temperature of the lower surface was measured with a thermocouple placed inside a narrow hole in the aluminium container. The accuracy is about 0.1 °C. In order to have an estimation of the temperature difference ΔT across the layer, we placed another thermocouple in the air over the liquid very close to it. Fixing this thermocouple to the probe, we positioned it within 10 μm of the surface.

The flow within the liquid is visualized using the classical shadowgraph method, which we have adapted to the specific geometry of our system. The cell is illuminated with a large parallel beam obtained by placing a small lamp in the focus of a spherical mirror. The mirror, along with a beam splitter, focus the light after the reflection on the bottom of the cell. By introducing a small astigmatism, the image is formed slightly out of the optical axis, and it is collected by a lens and a standard charge-coupled-device (CCD) camera. A knife edge is also introduced in the image focal plane in order to intercept the secondary images that result from multiple reflections on the beam splitter. This knife edge also enhances the contrast of the images. The camera is connected to a computer from which the experiment is monitored. It is worth noting that this system of visualization is highly nonlinear. In Fig. 2 some pictures obtained with this system are shown. The bright, thin lines that can be observed correspond to minima of the temperature field of the liquid. The cell boundaries, where liquid motion is downflow, can thus be sharply located.

III. EXPERIMENTAL RESULTS

The experimental procedure was the following. For each Γ we increase heating at a very slow rate until a pattern can be seen. Then we fix the heating input and let the system reach a steady state. When it remains stable for about 6 h we again increase the heat power by applying a small step. We wait again for equilibrium and observe the stable pattern. The procedure is repeated in five successive steps. The experimental results obtained for the different values of Γ considered are summarized in Fig. 3, where only stable patterns are reported. The measured temperature difference ΔT is of about 2 °C for the lowest heating and about 12 °C for the highest one. The corresponding values of the Marangoni and Rayleigh numbers for those values of ΔT are $M \cong 30$, $R \cong 600$ and $M \cong 150$, $R \cong 3000$, respectively, for an intermediate aspect ratio ($\Gamma = 6$). This shows that in our experiment buoyancy effects cannot be neglected.

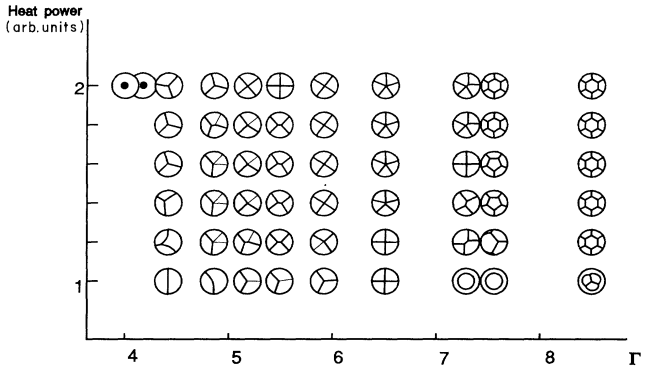

FIG. 3. Schematic representation of the stationary patterns observed in the experiments for different aspect ratios and heating. In the first two patterns, dark points correspond to upflow motions. In the rest of the patterns, cold lines are represented by solid lines.

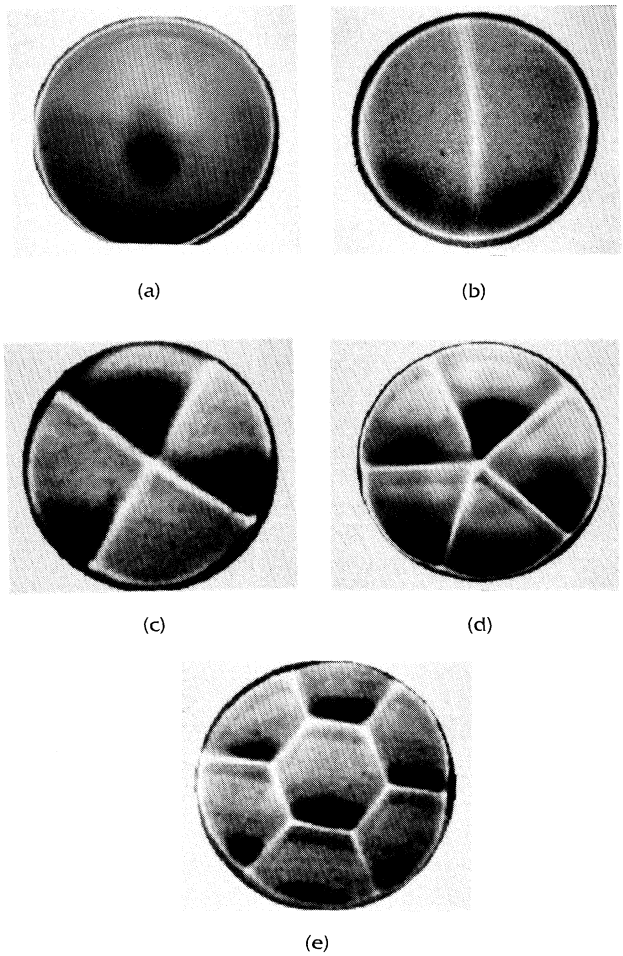

FIG. 2. Shadowgraphs of the stale patterns corresponding to simple modes [(a) $m = 0$, (b) $m = 2$, (c) $m = 4$, (d) $m = 5$] and to a single hexagon (e) that appear at the onset of convection. Bright lines correspond to the minimum of the temperature field where the liquid is sinking. The dark regions are due to the knife edge introduced in the optical system. (The lines are sightly shifted due to the knife edge.)

Considering the system behavior at the threshold point, it can be noticed that the patterns that show up strongly depend on Γ. For Γ smaller than 4.4 an axisymmetric pattern characterized by a hot point in the center of the cell and downflow near the sidewalls is observed [Fig. 2(a)]. In this case the motion of the fluid is toroidal. When Γ is increased, some patterns with azimuthal distribution can be seen: the cell is first divided in two by a cold line, and then in a symmetric partition in three or four cells [Figs. 2(b)–2(d)]. These patterns correspond to simple modes with radial wave number $i = 1$ and azimuthal wave number $m = 0$, 2, 3, and 4, respectively.

For Γ larger than 6.5, we observe an important change: the pattern is not constituted only by azimuthal nodal lines, but a radial partition begins to appear (the radial wave number i becomes equal to 2). We observe a cold circle as sketched in Fig. 3 for an aspect ratio $\Gamma = 7.2$ and 7.6. This corresponds to two concentric toroidal cells. For larger aspect ratios, we observe a partition inside the cold circle (Fig. 2, $\Gamma = 8.5$). This cold circle could be a subcritical pattern, as the one described by Koschmieder and Prahl [12] or to sidewall effects [16]. (Nevertheless we obtained in some simulations of a GSH equation a similar stable pattern that cannot be regarded as subcritical.) Starting from these patterns and increasing slightly the heat power, we get a pentagonal or hexagonal central cell surrounded by polygonal cells [Fig. 2(e)] in agreement with the statements explained in [16].

At threshold we thus observe an increase of the number of cells when Γ is increased, but the value of Γ for a given pattern differs from calculations of RDH. This fact has also been reported by Koschmieder and Prahl [12]. This could be due presumably to buoyancy effects, not considered by RDH, or to their unrealistic boundary conditions. However, for intermediate heat powers (1.4 and 1.6 in the scale of Fig. 3) the number of cells does not follow a monotonic variation with Γ. For example, we have five cells for $\Gamma = 6.5$ and again four cells for $\Gamma = 7.2$.

When increasing ϵ for a given Γ, we also see, for nearly

all the aspect ratios studied, a transition between modes. This is a confirmation of the existence of the higher instabilities predicted by RDH and allows one to study the competition between different modes. In our case, we observe that the transition always goes towards a pattern with a greater number of cells.

The transition between two modes occurring when we increase ϵ is almost never a direct transition (the only direct transition we observe is one from a pentagon to a hexagon, occurring at $\Gamma=7.6$); the system evolves through patterns that do not correspond to simple modes. We distinguish between two types of such patterns, which we call *nonsymmetrical patterns* and *mixed structures.* We have to emphasize that all those configurations are not transient stages. We verified this waiting sometimes for one or two days without noticing any remarkable change in the pattern. Moreover, we checked that those patterns are not due to an inclination or to defects of the cell.

A. Nonsymmetrical patterns

Some examples of these patterns are given in Fig. 4 in the case of partitions in $m=2$, 3, 4, and 5 cells. These figures have the same number of cells as simple modes but do not have its O_m symmetry.

Among these figures we can distinguish two different types of nonsymmetric patterns: in the cases where $m=2$ and 3 [Figs. 4(a) and 4(b)], the number of vertices remains unchanged with respect to the symmetrical case, but the pattern is not centered in the cell. With regard to the cases where $m=4$ and 5 [Figs. 4(c) and 4(d)], the original central vertex is split into two vertices of lower order: two vertices of order 3 for the case $m=4$, one of order 3 and one of order 4 for $m=5$. Note that these patterns cannot be described by a combination of a few modes.

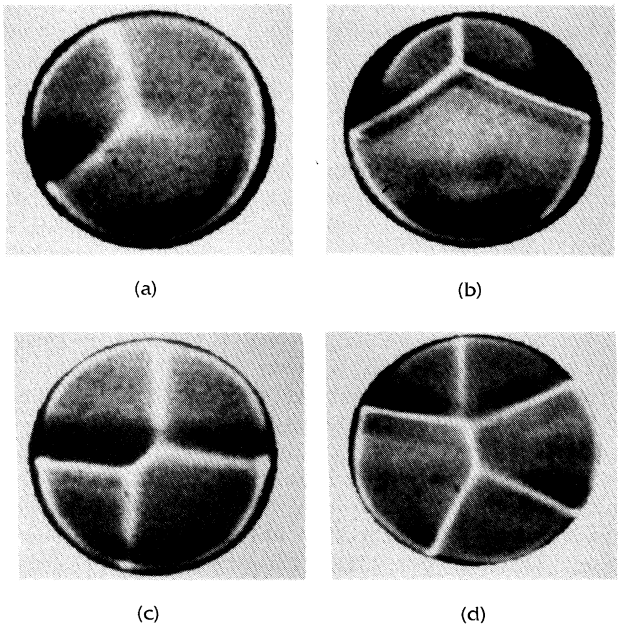

FIG. 4. Shadowgraphs of nonsymmetrical patterns.

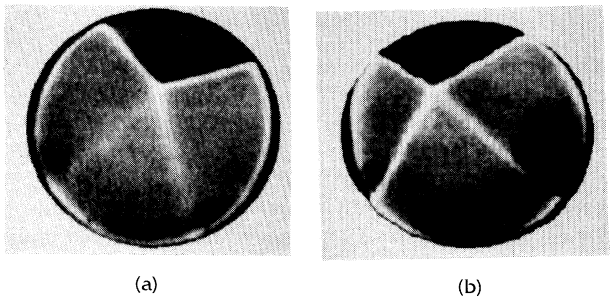

FIG. 5. Mixed structures: (a) two bright lines and two dim lines, (b) three bright lines and one dim line. These modes can be interpreted as a mixing of modes $m=3$ and 4.

B. Mixed structures

In all the configurations described above, all the cold lines have approximately the same intensity. This is not the case for some of the patterns observed. In the case of a partition in four cells, for instance, we obtain patterns with three bright lines and one weaker line, or two bright and two weak lines. Examples of these patterns are shown in Fig. 5. The fact that these patterns are observed when the mode changes from $m=3$ to 4 suggests that these are a linear combination of simple modes. We will call these patterns mixed structures. In order to test this conjecture, we have computed the temperature fields for the superposition of two simple modes. The results are shown in Fig. 6, where the contours correspond to isothermal (or isovelocity) lines. Quite a good correspondence is found between this superposition of simple modes and the mixed structures observed experimentally (compare Figs. 5 and 6). The angles between the different lines of the observed patterns are also comparable with those of Fig. 6. In the experiments, however, the structures are off-centered. A combination of $m=2$ and 3 modes is also found to be describable with the same procedure.

IV. NUMERICAL SIMULATIONS

It is difficult to perform a direct analysis of the hydrodynamic equations with real boundary conditions. Therefore, some simplified models are proposed. The amplitude equation approach can be derived within a weakly nonlinear analysis, but it considers only slow spatial variations with an imposed direction in the resulting pattern. A different approach is to derive a two-dimensional (2D) rotationally invariant equation for fast variables in which the natural symmetries of the system are included. This leads to the so-called generalized Swift-Hohenberg equations. Simulations of this kind of equations lead to patterns with characteristics similar to those observed in experiments, when appropriate boundary conditions are included. The interest of such simula-

tions is broadened by the fact that most of the patterns observed in experiments cannot be described in the amplitude equation framework.

Such a model, first proposed by Swift and Hohenberg [14], can be deduced directly from the basic equations that describe the problem with which we are dealing. This equation was successfully used to reproduce the patterns observed in small-aspect-ratio containers in Rayleigh-Bénard convection [17]. It was extended by Bestehorn and Haken [18] to study more general situations. The generalized Swift-Hohenberg equation proposed by these authors reads as

$$\dot{\Psi}=[\epsilon-(1+\Delta)^2]\Psi+\delta\Psi^2-\Psi^3 .$$

The field $\Psi(x,y,t)$ represents the local amplitude of the main convective variables (the temperature and vertical velocity) in a horizontal plane, and Δ is the two-dimensional Laplacian operator. The quadratic term accounts for the breaking of the symmetry on reflection through the midplane of the convective cell (due in our case to the surface-tension effects) [15,18]. The influence of temperature in the surface tension is thus included in the coefficient δ. The cubic term saturates the perturbation growth. The boundary conditions (BC's) for this equation that model rigid and insulating sidewalls are $\Psi=\partial_n\Psi=0$, where ∂_n is the derivative normal to the wall [16]. These conditions are not derived from the hydrodynamical equations, but they are proposed after some stringent approximations. Therefore, they can only be considered as a phenomenological approximation. However, these BC's lead to remarkably good results, as one can see in the reviews of Greenside and Coughran [17] and Friedrich, Bestehorn, and Haken [19], even in the case of small Γ.

We solved the GSH equation by an explicit finite-difference scheme as explained by Bjorstad *et al.* [20], first used by Greenside, Coughran, and Schryer [21]. The finite differences are evaluated on a mesh of 80×80 points, starting always from random initial conditions and applying directly a constant ϵ. This corresponds to a situation in which ΔT is suddenly increased above ΔT_c. In large-aspect-ratio containers, $\epsilon=0$ gives the neutral stability curve. For finite cells, however, convection is only stable for ϵ greater than a certain positive value because of the damping influence of the lateral walls. In the simulation we assume $\delta=1$.

Using these criteria, we first made several runs changing Γ. In Fig. 7 some of the patterns that have been ob-

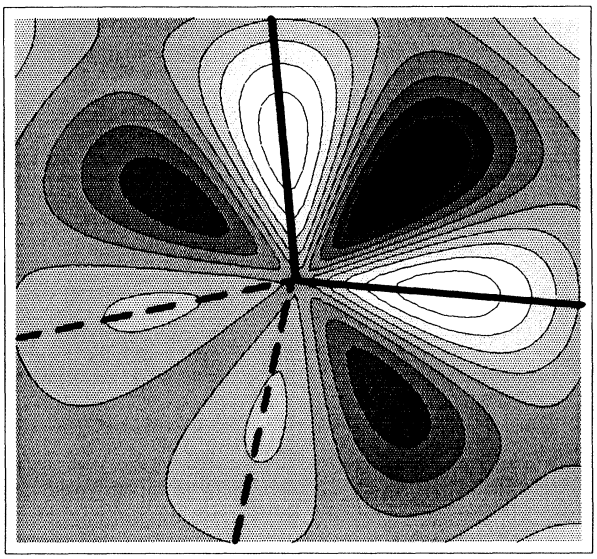

FIG. 6. Linear superposition of modes $m=3$ and 4 with two different phases. The contours show isovelocity lines. (These patterns are similar to those in Fig. 5.)

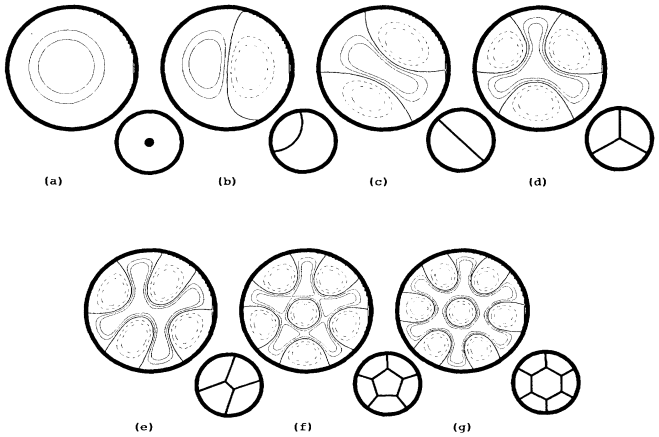

FIG. 7. Contour plots for stable amplitude field $\Psi(x,y)$. Five contour lines are drawn that correspond to $-M/2$, $-M/4$, 0, $M/4$, and $M/2$, where M is the maximum of Ψ. At the bottom right of each figure a drawing shows the pattern that would be seen with a shadow-graph system. Aspect ratios are (a) $\Gamma=2.4$, (b) $\Gamma=3.5$, (c) $\Gamma=3.8$, (d) $\Gamma=4.5$, (e) $\Gamma=5.7$, (f) $\Gamma=6.5$, and (g) $\Gamma=7.3$ ($\epsilon=0.5$).

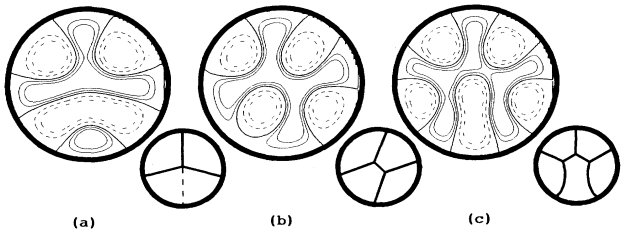

FIG. 8. Contour plots of nonsymmetric patterns. (a) $\Gamma=5.5$, $\epsilon=0.3$, (b) $\Gamma=5.8$, $\epsilon=0.3$, (c) $\Gamma=6$, $\epsilon=0.5$.

tained are shown. (In these figures the lines represent isotherms.) Regions inside solid lines represent the colder part of the fluid (downflow motions), while dotted contour lines represent the hotter parts (upflow motions). Some of them correspond to simple modes in the amplitude equation description [Figs. 7(a)–7(d)], but others cannot be obtained within that formalism [Figs. 7(e)–7(g)]. These latter correspond to larger aspect ratios for which we get a pentagonal or hexagonal cell in the middle of the container. A correspondence between the figures obtained in simulations and the experimental images can be established by locating the bottom of the valleys made by Ψ. These are the clear lines that are seen in shadowgraph images. A sketch of the image that one would actually see is shown along with each numerical result. It is interesting to notice that the patterns appear in the same order as in the experiments as Γ is increased, although the value of Γ for identical pictures is not exactly the same. In our case, this could be blamed to the particular values chosen for the coefficients of the Swift-Hohenherg equation, especially for δ. There is no simple way to connect these values to the experimentally accessible parameters.

Remarkably, the numerical simulations also give nonaxisymmetric patterns. These are not transients because the GSH equation with the BC has a Lyapunov functional and, therefore, the dynamics is purely relaxational. A rich variety of patterns can be obtained if Γ is chosen in such a way that the first unstable mode is not a simple mode. In Fig. 8 some of the patterns that we called *nonsymmetrical patterns* or *mixed structures* are reproduced. A competition between modes has been observed before the stationary pattern is reached.

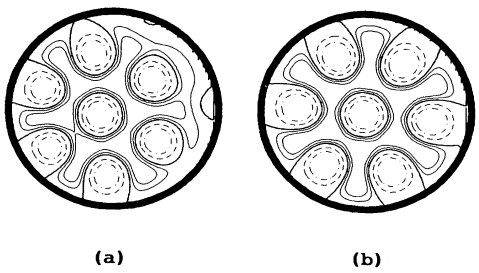

FIG. 9. The symmetry of the pattern is found to increase for higher ϵ. For these figures $\Gamma=7.5$. (a) $\epsilon=0.1$, (b) $\epsilon=0.3$.

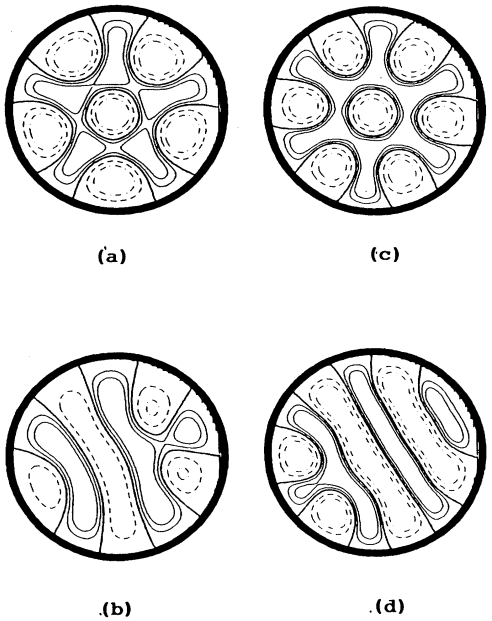

FIG. 10. When δ is decreased the roll solution is recovered. (a) $\Gamma=6.5$, $\delta=1$; (b) $\Gamma=6.5$, $\delta=0$; (c) $\Gamma=7.3$, $\delta=1$; (d) $\Gamma=7.3$, $\delta=0$. ($\epsilon=0.5$.)

Moreover, the GSH equation gives some information on the pattern dynamics:

(i) If ϵ is increased, the symmetry of the patterns is also higher. For example, a transition is observed for $m=6$ from a structure made up of six cells that is not centered in the container to an axisymmetric pattern when increasing supercriticality (Fig. 9). This has been verified experimentally.

(ii) A transition between the structures presented and a roll pattern can be obtained if δ is decreased, i.e., when decreasing surface-tension effects, and so results similar to those obtained by Greenside and Coughran [17] are recovered (Fig. 10). The role of surface tension is therefore dominant in the formation of the observed patterns.

(iii) The dynamics of the transition between modes can be studied. We thus observe that defects begin to grow near the wall and then move towards the center of the cell. This eventually leads to the formation of the new pattern. This process is confirmed by experimental observations.

V. CONCLUSIONS

The behavior of patterns in BM convection in small-aspect-ratio containers has been studied experimentally for different supercritical heatings and aspect ratios. An observed feature not described in previous experimental works is the appearance of nonaxisymmetric patterns. These can be of two kinds: (1) linear superposition of modes with different azimuthal number, and (2) purely nonsymmetrical patterns. The latter are difficult to describe in terms of the amplitude equations analyzed in theoretical works [10]. All those patterns are stationary

and some transitions can be characterized when ϵ is increased for a fixed Γ.

To complete the theoretical analysis, we use a generalized Swift-Hohenberg equation, including a quadratic term that accounts for the breaking of the vertical symmetry about the midplane of the fluid due to surface-tension dependence on temperature. In this equation the spatial dependence is explicitly introduced through Laplacian terms. The boundary conditions, crucial to take into account for small-aspect-ratio effects, are those used in most simulations, because they reproduce quite well rigid and insulating sidewalls. Numerical simulation of this model for small Γ yields patterns similar to that observed in the experiments. It is worth noting that the obtained patterns appear in the same order as in the experiments as Γ is increased, although the values are not exactly the same.

ACKNOWLEDGMENTS

We thank Mr. P. Elizalde for his help with the experiments. The authors also want to thank Dr. M. Bestehorn for his help in the numerical calculations and Dr. A. B. Ezersky for his suggestion about the use of the GSH model in this problem. Financial support for this work was provided by the Spanish Government (DGICYT OP90-0098, PB90-0362, and PB91-0627) and by the Gobierno de Navarra (OF 725/91). One of us (T.O.) also thanks the Ministerio de Educación (Spanish Government) for a research grant.

*Permanent address: Laboratoire de Physique de la Matière Condensée, Collège de France, 11 Place Marcelin Berthelot, F-75231 Paris CEDEX 05, France.

†Also at CITEFA/CONICET, 1603 Villa Martelli, Argentina and Universidad de San Luis, Chacabuco y Pedernera, 5700 San Luis, Argentina.

‡Also at Departament de Física Fonamental, Facultat de Física, Universitat de Barcelona, Avgda. Diagonal 647, 08028 Barcelona, Catalonia, Spain.

[1] D. A. Nield, J. Fluid Mech. **19**, 341 (1964).
[2] H. Bénard, Rev. Gen. Sci. Pure Appl. **11**, 1261 (1900).
[3] E. L. Koschmieder, J. Fluid Mech. **30**, 9 (1967).
[4] P. Cerisier, R. Ocelli, C. Pérez-García, and C. Jamond, J. Phys. (Paris), Colloq. **48**, C4-596 (1987).
[5] J. W. Scanlon and L. A. Segel, J. Fluid Mech. **30**, 149 (1969).
[6] A. Cloot and G. Lebon, J. Fluid Mech. **145**, 447 (1984).
[7] R. Ocelli, E. Guazzelli, and J. Pantaloni, J. Phys. Lett. **4**, L597 (1983).
[8] A. Libchaber and J. Maurer, J. Phys. Lett. **39**, L69 (1978).
[9] M. Dubois, M. A. Rubio, and P. Bergé, Phys. Rev. Lett. **51**, 1446 (1983).
[10] S. Rosenblat, S. H. Davis, and G. M. Homsy, J. Fluid Mech. **120**, 91 (1982).
[11] P. Cerisier, C. Pérez-García, C. Jamond, and J. Pantaloni, Phys. Lett. **112A**, 366 (1985).
[12] E. L. Koschmieder and S. A. Prahl, J. Fluid Mech. **215**, 571 (1990).
[13] A. B. Ezersky, A. D. Preobrazhensky, and M. I. Rabinovich, Eur. J. Mech. B **10**, 211 (1991).
[14] J. Swift and P. C. Hohenberg, Phys. Rev. A **15**, 319 (1977).
[15] H. Haken, *Advanced Synergetics* (Springer, Berlin, 1983).
[16] For a review on the sidewall effects in cylindrical containers, see M. Bestehorn and C. Pérez-García, Physica D **61**, 67 (1992) and references cited therein.
[17] H. S. Greenside and W. M. Coughran, Jr., Phys. Rev. A **30**, 398 (1984).
[18] M. Bestehorn and H. Haken, Phys. Lett. **99A**, 265 (1983).
[19] R. Friedrich, M. Bestehorn, and H. Haken, Int. J. Mod. Phys. B **4**, 365 (1990).
[20] P. Bjorstad, W. M. Coughran, Jr., H. S. Greenside, D. J. Rose, and N. L. Schryer, *Elliptic Problem Solvers II*, edited by G. Birkoff and A. Schoenstadt (Academic, New York, 1984).
[21] H. S. Greenside, W. M. Coughran, Jr., and N. L. Schryer, Phys. Rev. Lett. **49**, 726 (1982).

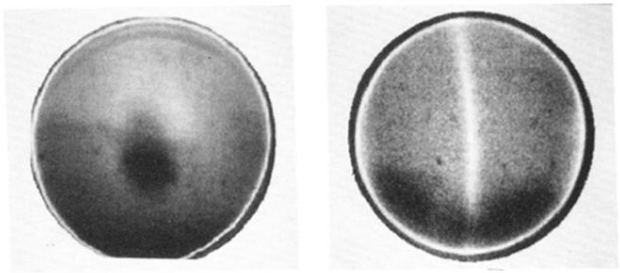

(a)

(b)

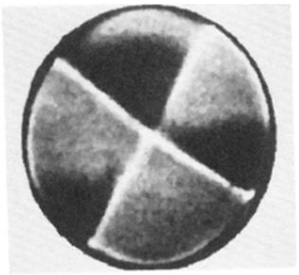

(c)

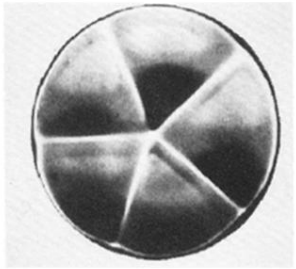

(d)

(e)

FIG. 2. Shadowgraphs of the stale patterns corresponding to simple modes [(a) $m=0$, (b) $m=2$, (c) $m=4$, (d) $m=5$] and to a single hexagon (e) that appear at the onset of convection. Bright lines correspond to the minimum of the temperature field where the liquid is sinking. The dark regions are due to the knife edge introduced in the optical system. (The lines are sightly shifted due to the knife edge.)

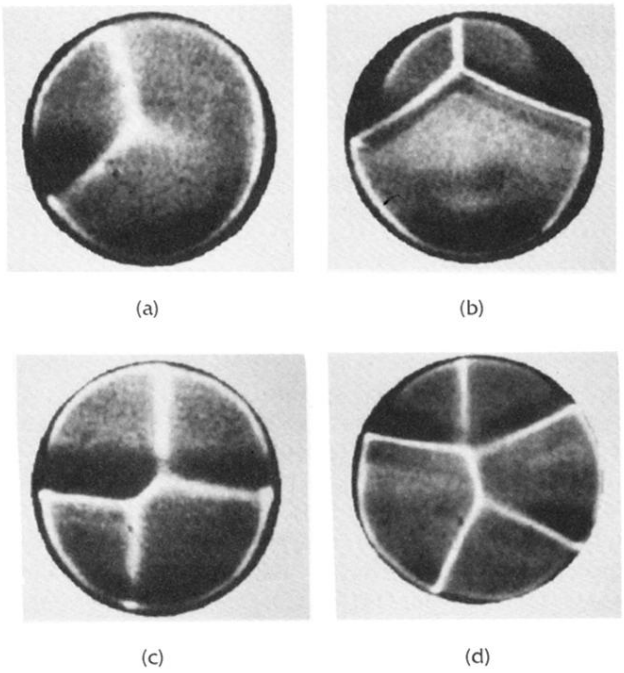

FIG. 4. Shadowgraphs of nonsymmetrical patterns.

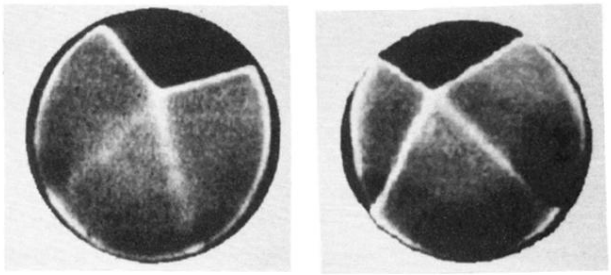

(a) (b)

FIG. 5. Mixed structures: (a) two bright lines and two dim lines, (b) three bright lines and one dim line. These modes can be interpreted as a mixing of modes $m = 3$ and 4.